JOURNAL OF MATERIALS SCIENCE **40** (2005) 4293–4298

Micro-Raman spectroscopy and X-ray diffraction studies of atomic-layer-deposited ZrO_2 and HfO_2 thin films

S. N. TKACHEV, M. H. MANGHNANI
School of Ocean and Earth Science and Technology, University of Hawaii, Honolulu, Hawaii, USA

A. NIILISK*, J. AARIK, H. MÄNDAR
Institute of Physics, University of Tartu, Riia 142, 51014 Tartu, Estonia
E-mail: niilisk@fi.tartu.ee

Raman spectroscopy and X-ray diffraction (XRD) methods were applied to characterize ZrO_2 and HfO_2 films grown by atomic layer deposition (ALD) on silicon substrates in chloride-based processes. A dramatic enhancement in spectral quality of Raman data resulted from the use of the film's freestanding edges for experimental runs between 80 and 800 cm^{-1}. Both techniques detected a preferential formation of a metastable phase in ZrO_2 and HfO_2 films at 500 and 600°C, respectively, during the initial stages of ALD. In the case of ZrO_2 films this phase was identified as the tetragonal polymorph of ZrO_2 (*t*-ZrO_2). XRD and Raman spectroscopy data showed that, in contrast to the monoclinic phase (m-ZrO_2), the absolute amount of t-ZrO_2 remained approximately constant while its relative amount decreased with the increase of the film thickness from 56 to 660 nm. Neither XRD nor Raman spectroscopy allowed unambiguous identification of the metastable phase formed in otherwise monoclinic HfO_2 films. © *2005 Springer Science + Business Media, Inc.*

1. Introduction

Zirconia (ZrO_2) and hafnia (HfO_2), dielectrics with similar chemical and physical properties, are of significant interest as promising high-*k* materials that could replace SiO_2 in microelectronics [1]. Thin films of these oxides, that possess a relatively wide band gap, high refractive index and high dielectric constant, are also considered for a variety of applications in optical coatings [2–5], gas sensors [6] and electronic devices [7–10].

At ambient conditions both oxides have stable monoclinic (*m*) structure [11–14] which transforms at high temperatures to a tetragonal (*t*) phase and then to a cubic (c) one [15, 16]. The *t*- and *c*-ZrO_2 and HfO_2 can also be stabilized in doped crystals [17, 18], nanostructured materials [19–24] and also in thin films [21, 25–27] at ambient conditions. In the nanostructured materials and thin films the small sizes of crystallites have been assumed to be responsible for stabilization of these phases [19, 20]. In addition, new orthorhombic (*o*) phases of ZrO_2 and HfO_2 have been observed at high pressures [28–30] and evidence of formation of the orthorhombic phase in HfO_2 thin films at low pressures has also been reported [31, 32].

Undeniably, the electrical and optical properties of thin films depend on their phase composition. Thus, the investigation and control of the structure development during the thin-film growth is very important. It is also obvious that, in addition to the film thickness that influences the crystallite sizes, the growth method and process parameters also contribute to the composition of thin films.

In the last few years, atomic layer deposition (ALD) has attracted an increasingly high interest as a prospective method in processing ultrathin ZrO_2 and HfO_2 films for the purposes of electronic industry [33] as well as for applications in optical coatings [34]. While there have been extensive studies of the crystallization occurring during ALD of the thinner ZrO_2 and HfO_2 films at relatively low temperatures [21, 24, 34, 35–38], there is an ambiguity in the identification of metastable phases in the thicker films [39–42]. Moreover, little information is available with regard to the structural processes in the ALD films grown at higher temperatures, that are especially important during the deposition, when low concentrations of impurities in the resulting product are needed [21, 23, 31, 35–37, 43]. Therefore, in the present work, we are testing the combination of XRD and Raman scattering techniques in order to find a reliable method to describe both the structure of ZrO_2 and HfO_2 films, grown at 500–600°C, and the phase transition, presumably taking place during ALD.

*Author to whom all correspondence should be addressed.

0022–2461 © *2005 Springer Science + Business Media, Inc.*

2. Experimental procedure

The ZrO_2 and HfO_2 thin films were grown in a low-pressure (250 Pa) flow-type ALD reactor described earlier [43]. We used $ZrCl_4$ and $HfCl_4$ as the metal precursors, and H_2O as the oxygen precursor. The transport gas was pure (99.999%) nitrogen. The growth process consisted of periodically repeated deposition cycles. Each cycle included a metal precursor pulse of 2 s, purge time of 1 s, oxygen precursor pulse of 1 s and another purge time of 2 s in duration. The number of growth cycles varied from 500 to 6000. The growth temperature was 500 and 600°C in the case of ZrO_2 and HfO_2 films, respectively. The corresponding growth rates were 0.11 and 0.096 nm per cycle. The ZrO_2 and HfO_2 films were grown onto the silicon, quartz glass, r-sapphire, and MgO substrates, simultaneously placed inside the growth reactor. In order to get more uniform HfO_2 films, HfO_2 buffer layers of 1 nm thickness were first grown at 300°C. No thermal post-annealing of films was performed. Some samples with Si substrates were subjected to the partial chemical etching in the HF:HNO_3 mixture in order to prepare freestanding areas (edges) of the film for subsequent micro-Raman measurements.

Present Raman studies were carried out using optical design similar to the one described in a previous paper [44]. The high quality spectra excited by Ar-ion laser (514.5 nm excitation wavelength and laser power of 5 to 10 mW on the sample with about 10 μm diameter laser spot in the focal plane) were recorded by a liquid nitrogen cooled CCD detector (1300 × 100 pixels) at room temperature in a backscattering geometry and processed by a PC-based software (WinSpec/32). The purity of the laser beam was improved by a bandpass filter used in conjunction with a 25 μm pinhole, which served as a spatial filter. Prior to passing the system of two notch filters and entering a 100 μm wide entrance slit of a fully automated imaging spectrometer TRIAX 550 (Instruments S.A., Inc., Jobin Yvon/Spex Division), a backscattered light was collimated by a long focal length objective lens (10×). A typical collection time was varying from 60 to 90 min. After subtracting a background scattering, the peak position, width and intensity of the Raman bands were estimated by peak fitting using a Lorentzian function.

A symmetrical Θ-2Θ powder XRD method was used for phase analysis and estimation of crystallite sizes in films. XRD data were collected on a diffractometer DRON-1 (vertical axis Bragg-Bretano geometry, Cu K_α radiation: 40 kV, 20 mA, incident (aperture 1.5°) and diffracted beam (aperture 2.5°) axial Soller slits, Ni K_β filter). Program AXES [45] was exploited for reflection detection, fitting and crystallite size determination. Diffractometer resolution function was measured on basis of SRM-660 (LaB_6). Physical width of reflections was determined by Voigt decomposition method as described earlier [46]. Apparent volume-weighted X-ray crystallite size $\langle D \rangle$ was estimated by well-known Scherrer equation

$$\langle D \rangle = \lambda(\beta \cos(\Theta))^{-1}$$

where λ is X-ray wavelength, β is physical width and Θ is Bragg angle for reflection.

In addition, the structure of some films was characterized using the high-energy electron diffraction (RHEED) method that was sensitive to the surface layer with the thickness of few nanometers. From these measurements additional information about the nucleation at the film surface was obtained.

3. Results and discussion

3.1. Raman scattering

Excellent quality Raman spectra (Fig. 1) were obtained when we had succeeded in using freestanding edges of thin films exposed after partial removal of Si substrates by etching. The corresponding Lorentzian-fitted band parameters (peak position, band width and relative intensity) are listed in Table I. The collection time did not depend on the film thickness and was 90 min for HfO_2 films and 60 min for ZrO_2 films. It is important to emphasize that no disturbing influence from characteristic Si line at 521 cm^{-1} [47] can be detected in our Raman spectra taken from a substrate-free area. The Raman band at 522 cm^{-1}, which exists in the HfO_2 spectrum, is about three times broader than the one for Si (in our experiments the full width at half maximum (FWHM) of Si peak was about 3 cm^{-1}), and, thus, can be firmly ascribed to HfO_2.

By contrast, strong Raman lines of the substrates (Si and sapphire) drastically limited the collection time and an intense continuous background scattering/luminescence (quartz glass and magnesia substrates) eclipsed weak Raman scattering of substrate-supported films. For this reason the spectra of substrate-supported ZrO_2 and HfO_2 films (without freestanding edges) will not be discussed in the present study.

The spectra of ZrO_2 and HfO_2 films have well-pronounced patterns (Fig. 1) of monoclinic structure. The Raman peak positions and width of the bands (Table I) are in good agreement with the values obtained earlier for bulk materials [12, 28]. The difference in the peak positions, which does not exceed 2–3 cm^{-1}

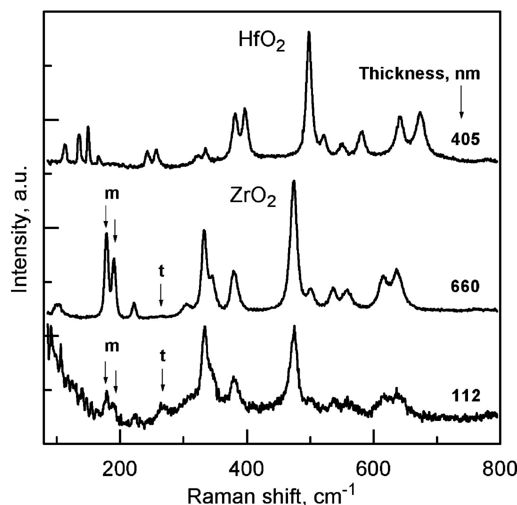

Figure 1 Raman spectra of ALD-grown HfO_2 and ZrO_2 films with various thicknesses. For ZrO_2, tetragonal (t) band at 265 cm^{-1} and monoclinic bands (m) at 179 and 190 cm^{-1}, utilized to estimate the tetragonality, are shown. Spectra are y-shifted for clarity.

TABLE I Raman band parameters

ZrO_2 ($d = 660$ nm) film			HfO_2 ($d = 405$ nm) film		
Peak position (cm^{-1})	Band width (cm^{-1})	Relative intensity (%)	Peak position (cm^{-1})	Band width (cm^{-1})	Relative intensity (%)
102	20.5	28	112	7.2	16.1
179	5.6	31.3	135	5.1	19.4
190	5.6	21	150	4.0	19.1
221	7.0	6.9	167	4.9	5.8
263	11.4	1.1	243	5.7	12.7
303	11.8	5.4	257	6.8	18.7
330	8.1	41.2	322	14.5	13.7
343	9.2	14.8	335	6.0	9.1
378	11.4	29.7	381	9.8	43.5
475	11.7	100	397	8.8	42.2
504	7.4	6.7	498	8.7	100
539	10.4	11.8	522	6.8	9.6
561	15.8	17.0	550	11.9	11.8
618	14.5	26.5	581	11.2	22.6
640	17.9	41.9	642	12.5	28.7
760	13.6	1.6	674	15.1	40.1
			776	35	14.1

for the more intense Raman bands, may partially be due to the experimental uncertainty of spectral calibration. There are no substantial discrepancies between the widths of Raman bands estimated at their half-maximum level after subtracting the background reflectance. The most significant differences can be seen in the relative intensities (areas) of bands. In the case of the films, some lower frequency bands have lower relative intensities in contrast to the same type of bands observed in single crystals or powders. These differences are probably due to the preferential orientation of crystallites revealed by XRD (see Section 3.2).

In the spectra of ZrO_2 films, a Raman band that can be attributed to the t-ZrO_2, occurs in the vicinity of 265 cm^{-1} (Fig. 1). The relative intensity of the peak increases with decreasing film thickness. Thus, the Raman spectroscopy data indicate that the relative amount of t-ZrO_2, T, increases with the decrease of film thickness. The value of T for a mixture of t- and m-ZrO_2 can be estimated using an empirical formula [48, 49]

$$T = I(265)/[I(265) + I(179) + I(190)]$$

where $I(265)$, $I(179)$, and $I(190)$ are the intensities of corresponding Raman bands. The result of this estimation is displayed in Fig. 2 with T as a function of film thickness. Due to the low intensity of the 265 cm^{-1} band the calculated points scatter noticeably. Moreover, it was impossible to get substrate-free samples of the thinnest, 56-nm ZrO_2 film because it was too fragile to retain free-standing edges sufficient for Raman measurements. Nevertheless, one can see that although the relative amount of t-ZrO_2 is negligible in the thicker film, it increases rapidly with decrease in the film thickness and reaches 40–50% for 112 nm film, the thinnest film studied by Raman spectroscopy.

The absolute amount of t-ZrO_2 calculated, assuming the 100% crystallinity of the films, decreases by the factor of 1.20 ± 0.15, when the film thickness is increased from 56 to 112 nm, and is only slightly de-

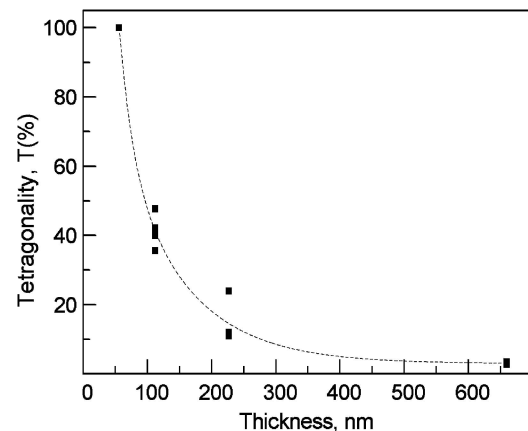

Figure 2 Concentration of tetragonal phase vs. film thickness for ZrO_2 on Si(111) substrate as estimated from the Raman spectra. 100% tetragonality value is obtained by XRD measurements (see Fig. 3)

creasing with further thickness increase. Thus, tetragonal phase, once formed during the initial stage of ALD, is partially transforming to a monoclinic structure until the film gets thicker than 112 nm. After that the rest of t-ZrO_2 remains practically unaltered at the bottom of the film. Although in some experiments, the growth duration reached 10 h, there was no distinct t-ZrO_2 to m-ZrO_2 phase transition observed during the ALD of the film thicker than 112 nm at temperatures as high as 500°C. RHEED studies, which are sensitive to a thin outermost layer of a film, have also demonstrated that t-ZrO_2 can be obtained in the initial stage of ALD growth at this temperature. Nucleation of m-ZrO_2 is initiated at the film thickness of 30 nm [50] and no noticeable crystallization of t-ZrO_2 occurs, when the film thickness exceeds 100 nm.

3.2. XRD analysis

Diffraction patterns of three ZrO_2 films with thickness of 660, 112 and 56 nm are shown in Fig. 3. The thickest (660 nm) film shows only reflections associated

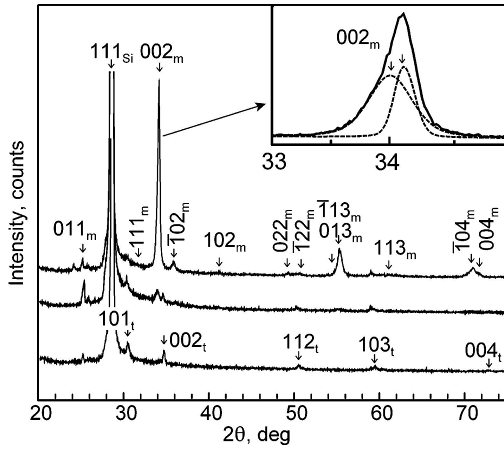

Figure 3 XRD patterns of ZrO_2 films on Si(111) substrate with thickness of 56 nm (lower), 112 nm (central), and 660 nm (upper curve). Subscripts *t* and *m* at the Miller indices denote reflections from tetragonal and monoclinic phases, respectively. Inset demonstrates asymmetry of the reflection 002_m from the thickest film (solid line). Fitting components (dashed lines) that can explain the reflection asymmetry are also shown.

TABLE II Apparent crystallite size $\langle D \rangle$ for ZrO_2 and HfO_2 films in different crystallographic directions

		Crystallic size (nm)				
Film	Thickness (nm)	$[101]_t$	$[001]_t$	$[001]_m$	$[010]_m$	$[100]_m$
ZrO_2	56	24(3)	44(4)	–	–	–
	112	19(2)	44(4)	16(2)	–	–
	227	–	–	16(2)	–	–
	660	–	–	25(3)	–	–
HfO_2	140	–	–	40(4)	56(6)	86(9)
	405	–	–	61(6)	84(8)	134(13)

Subscripts *t* and *m* denote tetragonal and monoclinic phases, respectively.

with m-ZrO_2 (space group $P2_1/c$, cell parameters $a = 0.511(3)$ nm, $b = 0.518(3)$ nm, $c = 0.5324(3)$ nm, $\beta = 99.24(5)°$), except for a very weak reflection at $d = 0.2944$ nm, which might belong to c-ZrO_2 (111) (space group Fm $\bar{3}$m), t-ZrO_2 (101) (space group $P4_2$/nmc) as well as o-ZrO_2 (211) (space group Pbca). The reflection is, however, not strong enough to get reliable data about the amount of these phases in the film.

Films with thickness 112 and 227 nm show reflections from two crystalline phases: m-ZrO_2 and the metastable tetragonal phase. All reflections from 56 nm thick film can be attributed to t-ZrO_2. Thus, ZrO_2 films are clearly undergoing almost complete gradual phase transformation from t-ZrO_2 to m-ZrO_2 with the increase in the film thickness (Fig. 3).

In all cases the most intense reflections are of type 00*l*. This indicates that crystallites grow preferentially in crystallographic direction [001] for both phases. Interestingly, in the case of the thickest (660 nm) film, reflection 002_m exhibits strong asymmetry at a lower angle side. The asymmetry can not be explained by contribution of reflections 020 and 200 of monoclinic phase because their calculated (from refined cell parameters of the monoclinic phase) locations at 34.58° and 35.87° are too far from the asymmetric reflection at 34.00°. A more reasonable explanation for the asymmetry is a slight variation of cell parameters (corresponding to the increase of *c* from 0.5324(3) nm to 0.5344(3) nm). The variation of the cell parameters may be due to non-uniform strain in the thicker films.

The XRD analysis has also revealed (Table II) that apparent crystallite sizes of t-ZrO_2 (directions [101] and [001]) and m-ZrO_2 (direction [001]) do not considerably vary with the change in film thickness from 56 to 112 and from 112 to 227 nm, respectively. An increase of the apparent mean crystallite size to 25 nm (calculated for m-ZrO_2) has been observed only for the thickest film. The asymmetry of the 002_m reflection (Fig. 3, inset), might also be related to the growth of larger crystallites, which have evidently a different intrinsic strain than the smaller crystallites do. At the same time small crystallites are evidently represented in the thickest film too. Thus, the co-existence of crystallites of different sizes can be proposed as another possible reason for the variation of cell parameters in the thickest film.

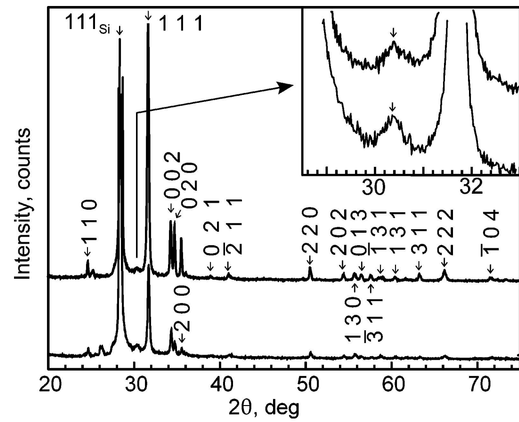

Figure 4 Diffraction patterns of HfO_2 films grown on Si(111) substrates at 600°C with 140 nm (lower) and 405 nm (upper) thickness. Subscript Si at a Miller index denotes reflection from silicon substrate. Indices without subscripts belong to monoclinic HfO_2. Inset at the upper right corner shows a weak reflection at 30.34°(see Section 3.2).

All reflections from HfO_2 films grown at 600°C (Fig. 4) have been attributed to a monoclinic system, except for one weak reflection at 30.34° ($d = 0.2944$ nm), which is consistent with the presence of such metastable phases as c-, t- or o- HfO_2. This weak reflection has approximately the same intensity for both thin (140 nm) and thick (405 nm) films, indicating that nucleation and growth of the metastable phase predominantly occur during initial stage of the ALD process.

Relative intensities of the reflections 002, 020 and 200 of m-HfO_2 in films are approximately the same as in a non-textured powder sample. However, it is clear (Table II) that the crystallite size in [100] direction is about 2 times larger than in the other directions. Therefore, [100] can be considered as a preferred crystallite size growth direction at 600°C.

XRD patterns of the thickest ZrO_2 and HfO_2 films studied in this work demonstrate that approximately similar amounts of the metastable phase have been formed in the films. The Raman spectroscopy measurements independently confirm the XRD data on ZrO_2 films and unambiguously show formation of metastable

t-ZrO_2 polymorph. In the case of HfO_2 films, however, the question of whether the metastable phases of HfO_2 (c, t or o, if any) are present in these films, still remains open and needs further clarification.

4. Conclusions

The Raman spectroscopy and XRD methods have been applied to characterize ZrO_2 and HfO_2 films grown by ALD on silicon substrates in chloride-based processes. In order to increase the sensitivity of the Raman spectroscopy method, the substrates have been partially removed by wet etching, and micro-Raman studies have been performed on freestanding edges of the thin films in the spectral range of 80–800 cm^{-1}.

The obtained results demonstrate that t-ZrO_2 is preferentially formed during the initial stage of atomic layer deposition. The concentration of t-ZrO_2 have appeared to be close to 100% for the films grown as thick as 56 nm at 500°C. Both XRD and Raman spectroscopy data show that while the absolute amount of t-ZrO_2 remains almost constant the relative amount of this phase decreases with the increase in the film thickness.

According to XRD data, the HfO_2 films grown at 600°C might also contain some traces of a metastable (c, t or o) phase in addition to the dominating m-HfO_2. It was impossible to determine the structure of the metastable polymorph due to its low concentration.

Acknowledgements

The authors are grateful to Mr. J. Balogh from Hawaii Institute of Geophysics and Planetology, Dr. S. Marsillac and Dr. E. Miller from the Thin Films Laboratory at Hawaii Natural Energy Institute, and Dr. A. Aidla, Dr. T. Uustare, Mrs. A.-A. Kiisler, and Mr. A. Kasikov from the University of Tartu for technical assistance. A.N. would like to thank the University of Hawaii for the fellowship. The work was partially supported by the Estonian Science Foundation (Grant No. 5861 and 3999).

References

1. A. C. JONES and P. R. CHALKER, *J. Phys. D: Appl. Phys.* **36** (2003) R80.
2. S. M. EDLOU, A. SMAJKIEWICZ and G. A. AL-JUMAILY, *Appl. Opt.* **32** (1993) 5601.
3. A. J. WALDORF, J. A. DOBROWOLSKI, B. T. SULLIVAN and L. M. PLANTE, *ibid.* **32** (1993) 5583.
4. M. GILO and N. CROITORU, *Thin Solid Films* **350** (1999) 203.
5. M. ALVISI, M. DI GIULIO, S. G. MARRONE, M. R. PERRONE, M. L. PROTOPAPA, A. VALENTINI and L. VASANELLI, *ibid.* **358** (2000) 250.
6. S. CAPONE, G. LEO, R. RELLA, P. SILICIANO, L. VASANELLI, M. ALVISI, L. MIRENGHI and A. RIZZO, *J. Vac. Sci. Technol. A* **16** (1998) 3564.
7. T. NGAI, W. J. QI, R. SHARMA, J. FRETWELL, X. CHEN, J. C. LEE and S. BANERJEE, *Appl. Phys. Lett.* **76** (2000) 502.
8. M. HOUSSA, V. V. AFANAS'EV, A. STESMANS and M. M. HEYNS, *ibid.* **77** (2000) 1885.
9. W. J. QI, R. NIEH, B. H. LEE, L. KANG, Y. JEON and J. C. LEE, *ibid.* **77** (2000) 3269.
10. B. H. LEE, L. KANG, R. NIEH, W. J. QI and J. C. LEE, *ibid.* **76** (2000) 1926.
11. E. ANASTASSAKIS, B. PAPANICOLAOU and I. M. ASHER, *J. Phys. Chem. Solids* **36** (1975) 667.
12. P. E. QUINTARD, P. BARBÉRIS, A. P. MIRGORODSKY and T. MERLE-MÉJEAN, *J. Am. Ceram. Soc.* **85** (2002) 1745.
13. B. BONDARS, G. HEIDEMANE, J. GRABIS, K. LASCHKE, H. BOYSEN, J. SCHNEIDER and F. FREY, *J. Mater. Sci.* **30** (1995) 1621.
14. R. RUH and P. W. R. CORFIELD, *J. Am. Ceram. Soc.* **53** (1970) 126.
15. G. TEUFER, *Acta Crystallogr.* **15** (1962) 1187.
16. S. BLOCK, J. A. H. DA JORNADA and G. J. PIERMARINI, *J. Am. Ceram. Soc.* **68** (1985) 497.
17. H. FUJIMORI, M. YASHIMA, S. SASAKI, M. KAKIHANA, T. MORI, M. TANAKA and M. YOSHIMURA, *Chem. Phys. Letters* **346** (2001) 217.
18. I. KOSACKI, V. PETROVSKY, H. U. ANDERSON and P. COLOMBAN, *J. Am. Ceram. Soc.* **85** (2002) 2646.
19. R. C. GARVIER, *J. Phys. Chem.* **82** (1978) 218.
20. M. A. SCHOFIELD, C. R. AITA, P. M. RICE and M. GAJDARDZISKA-JOSIFOVSKA, *Thin Solid Films* **326** (1998) 106.
21. K. KUKLI, K. FORSGREN, J. AARIK, T. UUSTARE, A. AIDLA, A. NISKANEN, M. RITALA, M. LESKELÄ and A. HÅRSTA, *J. Cryst. Growth* **231** (2001) 262.
22. T. MERLE, R. GUINEBRETIÈRE, A. MIRGORODSKY and P. QUINTARD, *Phys. Rev. B* **65** (2002) 144302.
23. J. AARIK, A. AIDLA, H. MÄNDAR, T. UUSTARE and V. SAMMELSELG, *Thin Solid Films* **408** (2002) 97.
24. M. CASSIR, F. GOUBIN, C. BERNAY, P. VERNOUX and D. LINCOT, *Appl. Surf. Sci.* **193** (2002) 120.
25. I. A. EL-SHANSHOURY, V. A. RUDENKO and I. A. IBRAHIM, *J. Amer. Ceram. Soc.* **53** (1979) 264.
26. A. MEHNER, H. KLÜMPER-WESTKAMP, F. HOFFMANN and P. MAYR, *Thin Solid Films* **308/309** (1997) 363.
27. J. SUNDQVIST, A. HÅRSTA, J. AARIK, K. KUKLI and A. AIDLA, *ibid.* **427** (2003) 147.
28. A. JAYARAMAN, S. Y. WANG, S. K. SHARMA and L. C. MING , *Phys. Rev. B* **48** (1993) 9205.
29. J. M. LEGER, P. E. TOMASZEWSKI, A. ATOUF and A. S. PEREIRA, *ibid.* **47** (1993) 14075.
30. J. M. LEGER, A. ATOUF, P. E. TOMASZEWSKI and A. S. PEREIRA, *ibid.* **48** (1993) 93.
31. J. AARIK, A. AIDLA, A.-A. KIISLER, T. UUSTARE and V. SAMMELSELG, *Thin Solid Films* **340** (1999) 110.
32. C. WIEMER, S. FERRARI, M. FANCIULLI, G. PAVIA and L. LUTTEROTTI, *ibid.* **450** (2004) 134.
33. O. SNEH, R. B. CLARK-PHELPS, A. R. LONDERGAN, J. WINKLER and T. E. SEIDEL, *ibid.* **402** (2002) 248.
34. S. ZAITSU, S. MOTOKOSHI, T. JITSUNO, M. NAKATSUKA and T. YAMANAKA, *Jpn. J. Appl. Phys.* **41** (2002) 160.
35. E. BONERA, G. SCAREL and M. FANCIULLI, *J. Non-Crystalline Solids* **322** (2003) 105.
36. G. SCAREL, S. FERRARI, S. SPIGA, C. WIEMER, G. TALLARIDA and M. FANCIULLI, *J. Vac. Sci. Technol. A* **21** (2003) 1.
37. G. SCAREL, C. WIEMER, S. FERRARI, G. TALLARIDA, and M. FANCIULLI, *Proc. Estonian Acad. Sci. Phys. Math.* **52** (2003) 308.
38. D. M. HAUSMANN and R. G. GORDON, *J. Cryst. Growth* **249** (2003) 251.
39. M. RITALA, M. LESKELÄ, L. NIINISTÖ, T. PROHASKA, G. FRIEDBACHER and M. GRASSERBAUER, *Thin Solid Films* **250** (1994) 72.
40. K. KUKLI, M. RITALA and M. LESKELÄ, *Chem. Vap. Deposition* **6** (2000) 297.
41. K. KUKLI, M. RITALA, T. SAJAVAARA, J. KEINONEN and M. LESKELÄ, *Thin Solid Films* **416** (2003) 72.
42. M. PUTKONEN, J. NIINISTÖ, K. KUKLI, T. SAJAVAARA, M. KARPPINEN, H. YAMAUCHI and L. NIINISTÖ, *Chem. Vap. Deposition* **9** (2003) 207.
43. J. AARIK, A. AIDLA, H. MÄNDAR, V. SAMMELSELG and T. UUSTARE, *J. Cryst. Growth* **220** (2000) 105.

44. A. F. GONCHAROV, V. V. STRUZHKIN, R. J. HEMLEY, H.-K. MAO and Z. LIU, in: "Science and Technology of High Pressure, Proceedings of AIRAPT-17," edited. by M. H. Manghnani, W. J. Nellis and M. F. Nicol (Universities Press, Hyderabad, India, 2000) p. 90.
45. H. MÄNDAR, J. FELSCHE, V. MIKLI and T. VAJAKAS, *J. Appl. Cryst*. **32** (1999) 345.
46. J. MALEK, L. BENES and T. MITSUHASHI, *Powder Diffraction* **12/2** (1997) 96.
47. M. CARDONA, "Light Scattering in Solids II," (Springer, Berlin, 1990).
48. P. BARBÉRIS, T. MERLE-MÉJEAN and P. QUINTARD, *J. Nucl. Mater.* **246** (1997) 232.
49. D. R. CLARKE and F. ADAR, *J. Am. Ceram. Soc*. **65** (1982) 284.
50. K. KUKLI, M. RITALA, J. AARIK, T. UUSTARE and M. LESKELÄ, *J. Appl. Phys.* **92** (2002) 1833.

Received 30 April 2004
and accepted 4 April 2005